Pergamon

Journal of Structural Geology, Vol. 17, No. 5, pp. 689 to 707, 1995

0191-8141/95 $9.50 + 0.00

0191-8141(94)00093-X

Development of phyllonite from granodiorite: Mechanisms of grain-size reduction in the Santa Rosa mylonite zone, California

LAUREL B. GOODWIN

Department of Geoscience, New Mexico Tech, Socorro, NM 87801, U.S.A.

and

HANS-RUDOLF WENK

Department of Geology and Geophysics, University of California at Berkeley, Berkeley, CA 94720, U.S.A.

(*Received* 20 *January* 1994; *accepted* 5 *August* 1994)

Abstract—Field and laboratory investigations indicate that phyllonite within the Santa Rosa mylonite zone developed from granodiorite without hydrous alteration of the original mineral assemblage. Initial grain-size reduction within zones of phyllonite was accomplished through whole-rock cataclasis; subsequent deformation occurred through ductile flow. The original cataclastic failure is recorded by sharp boundaries with the surrounding rock, which are retained through the ductile overprint.

Biotite in phyllonite has a mean grain size of ~3 μm and exhibits straight boundaries and a strong crystallographic preferred orientation. Trace analyses of HVEM images indicate that the largest biotite grains are most strongly oriented, and the grains are elongate parallel to lineation. TEM observations indicate that typical grains have irregularly spaced stacking faults and twins. Evidence for intracrystalline folding and cataclasis, present in protomylonite and mylonite, is absent; bending or kinking of grains is rare. These observations suggest that biotite in phyllonite accommodated deformation through dynamic recrystallization in concert with intracrystalline slip and mechanical rotation. Grain-size reduction to form phyllonite is accompanied by macroscopically and microscopically visible changes in the character of foliations in the rock. We suggest that these changes are linked to the deformation mechanisms operating within the fine-grained phyllonite.

INTRODUCTION

"I once deformed a thymol specimen which first yielded brittlely to produce a cataclasite and then transformed itself, by plastic deformation of the fragments, dynamic recrystallization and void-healing into a mylonitic material. This recalls the brittle-to-plastic history for shear zones in granite as interpreted by Segall and Simpson (1986), and reminds us again that some microstructures in rocks may have short memories of complex histories."

W. D. Means (1989)

Interest in mylonites and the process of mylonitization has grown over the past two decades with the recognition that mylonite zones are the deep crustal equivalents of shallow brittle faults, and that the entire brittle-to-ductile shear systems accommodate major deformations of continental crust (see reviews by Kirby 1985, Sibson 1986). Mylonites are generally understood to be the product of high strain, distinguished by three characteristics: (1) reduction in grain size from the protolith, (2) development of a strong foliation and/or lineation, and (3) confinement to a discrete zone (Tullis *et al.* 1982). Localization of strain within a discrete zone may be accomplished through a number of processes (see reviews by White *et al.* 1980, Kirby & Kronenberg 1987), among which mechanical weakening and reaction softening are most commonly documented. The importance of initial brittle structures in localizing strain (Segall & Simpson 1986, Tullis *et al.* 1990) is less well understood, perhaps in part due to the general rejection of the original idea that mylonites developed solely through cataclasis (Lapworth 1885), and in part because evidence of early brittle deformation is likely to be effectively erased during later plastic flow (cf. Means 1989, Tullis *et al.* 1990).

Preservation of structures developed during the early history of a mylonite zone depends on a heterogeneous distribution of strain throughout its development. Heterogeneous deformation within the Santa Rosa mylonite zone, California, allowed different steps in the process of mylonitization to be recorded; therefore, a full deformational history for the zone can be established. The bulk of the Santa Rosa mylonite zone is a granodiorite mylonite, with phyllonite and, rarely, ultramylonite locally present. Processes by which strain was localized within the narrow zones of phyllonite and ultramylonite are the primary focus of this paper. We present evidence that this localization was accomplished largely by reduction of grain size through initial cataclasis, and emphasize that this was achieved without the changes in mineralogy and bulk chemistry that typically accompany retrogression.

In the following text, we describe the structural features of the Santa Rosa mylonite zone from the large to

the small scale, focusing on the development of phyllonite. We note macroscopic and microscopic changes in the character of foliations that accompany this development, and suggest that changes in foliations reflect the changes in deformation mechanisms that occur with grain-size reduction.

REGIONAL SETTING

Two major shear zones cut the northern Peninsular Ranges batholith of southern California (Todd *et al.* 1988). The easternmost of these, the eastern Peninsular Ranges mylonite zone (Sharp 1979) extends from the latitude of Palm Springs southward for about 80 km (Fig. 1). Strands of the still-active San Jacinto Fault zone (Sharp 1967) divide the Eastern Peninsular Ranges mylonite zone into three segments from south to north; this paper is focused on the northernmost Santa Rosa mylonite zone.

Previous workers (Sharp 1979, Erskine 1985) have mapped the boundary between the granodiorite protolith and the Santa Rosa mylonite zone and identified a series of imbricate, low-angle faults (generally dipping less than 30° to the northeast; Fig. 1). Movement within this system of kinematically related mylonites and faults

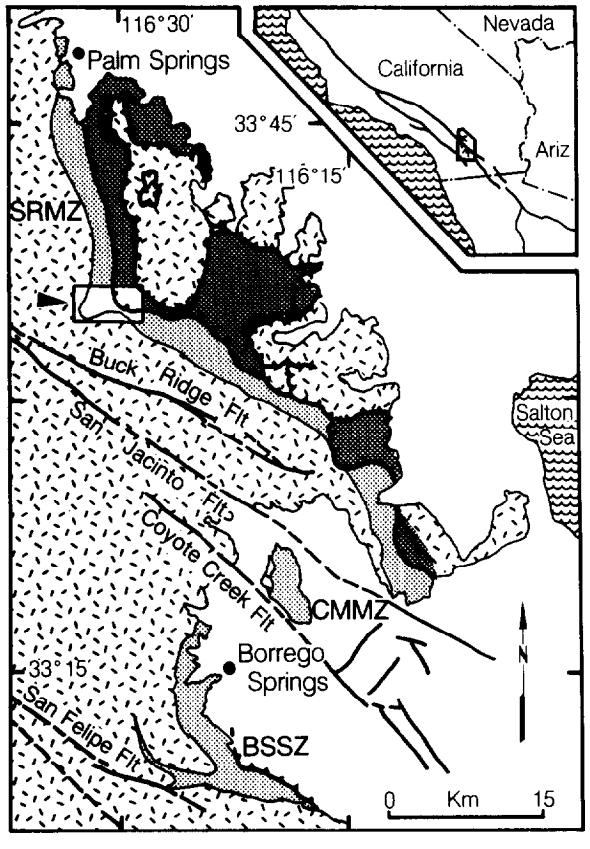

Fig. 1. Generalized geologic map of the eastern Peninsular Ranges mylonite zone (modified after Sharp 1979, Erskine 1985). Stippled pattern represents middle Cretaceous granitic rocks of the Peninsular ranges batholith and older included metasedimentary screens. Shading indicates mylonites. SRMZ = Ranta Rosa mylonite zone, CMMZ = Coyote Mountain mylonite zone, BSSZ = Borrego Springs shear zone. Barbed lines show positions of low-angle faults; barbs face the hanging walls. Bold lines show high-angle, predominantly strike-slip faults. The area of the detailed map shown in Fig. 2 is indicated by the box marked by an arrow.

was essentially top-to-the-southwest, indicating that it is a thrust system. Evidence for this comes independently from several workers and includes: (1) orientations of macroscopic structures within the footwall of the Santa Rosa fault (Sharp 1979); (2) petrographic analysis of sense-of-shear indicators in the mylonite zone (Simpson 1984); (3) geometric relations between individual low-angle faults and concordance of lineations on fault surfaces with the mylonitic lineation (Erskine 1985, 1986b); and (4) calculation of pressures of pluton crystallization (Ague & Brimhall 1988) using the hornblende geobarometer of Hammarstrom & Zen (1988). Ague and Brimhall suggest tectonic transport of as much as 5–7 km vertically along the system of mylonites and thrusts based on crystallization of the granodiorite protolith at pressures of 450 MPa (17 km depth) and of the Asbestos Mountain granodiorite above the uppermost thrust at 600–650 MPa (22–24 km depth). The former crystallization pressures are consistent with those of mineral assemblages of rocks from lower plate metasedimentary screens (Theodore 1970) in the Coyote Mountain mylonite zone (Fig. 1).

Mylonitization was initiated by ~80 Ma, with emplacement of the uppermost thrust sheets by ~60 Ma (Goodwin & Renne 1991). Crustal thickening resulted from thrusting in the Santa Rosa mylonite zone, so compression at right angles to the shear zone margins is probable. Quartz and calcite textures indicating a component of flattening during mylonitization have been noted by Erskine (1985) and Erskine & Wenk (1985). In addition, Erskine (1985, 1986a) and Todd *et al.* (1988) have postulated limited Cenozoic reactivation of Mesozoic thrusts on the basis of structures and petrologic trends suggesting eastward-directed movement along these faults. Reactivation of these thrust faults as low-angle normal faults is supported by fission track data (Dokka 1984; B. G. Erskine, personal communication 1989) that suggest rapid exhumation at ~60 Ma, immediately following the final phase of compressional deformation (Goodwin & Renne 1991).

A number of workers (Theodore 1970, Sharp 1979, Anderson 1983, Erskine 1985, 1986b, Todd *et al.* 1988) have suggested that intrusion of the eastern Peninsular Ranges batholith was syntectonic with respect to mylonitization. This assertion is based upon: (1) amphibolite grade metamorphism of rocks of the Coyote Mountain mylonite zone and the Borrego Springs shear zone (cf. Fig. 1), (2) rough concordance between the long dimensions of plutons, the strikes of deformation belts, and strikes of magmatic and mylonitic foliation, and (3) macroscopic structural features. However, field evidence and microstructural analysis (Simpson 1985, this paper) and the tectonothermal history of the zone (Goodwin & Renne 1991) indicate that mylonitization was initiated in holocrystalline plutonic rock.

Regionally, the metamorphic grade in metasedimentary screens in the Peninsular Ranges batholith rises from greenschist facies in the west to amphibolite facies in the east (Fig. 3 of Todd *et al.* 1988). Evaluation of a cooling curve in light of the tectonic history of the Santa

Rosa mylonite zone indicates that mylonitization must have been initiated before the rocks cooled to 330°C (Goodwin & Renne 1991); microstructural analysis of the granodiorite mylonite suggests that the zone deformed mainly at middle amphibolite facies conditions (Simpson 1985). Recrystallized plagioclase within the mylonite zone has a composition of An_{30-35} (Ague 1988), consistent with amphibolite facies conditions.

STRUCTURAL VARIATION

Terminology

In the region of study (Figs. 1 and 2) the mylonite zone is developed largely in plutonic rocks of the Peninsular Ranges batholith. Included metasedimentary screens are rare and are not considered here. The area contains the hinge of a broad, gentle fold in the mylonite zone; the fold appears to have developed during mylonitization with a fold axis parallel to the mylonitic lineation (Erskine 1985). Three structural domains (Fig. 2) were delineated in the field on the basis of macroscopic structures within the zone. These structures, field relations and petrographic observations are described in later sections. Terminology in this description follows Sibson (1977): a protomylonite is distinguished by 10–50% matrix formed by grain-size reduction, a mylonite has 50–90% matrix, and an ultramylonite contains 90–100% matrix. The term phyllonite, introduced by Sander (1911), is a contraction of 'phyllite mylonite' and indicates a rock of phyllitic appearance which was created through deformation. Knopf (1931) enlarged on this definition, pointing out that "... this means a phyllite produced by mylonitization of an originally coarser-grained rock" and "Although many phyllonites are diapthoritic [the product of retrogression] they are not necessarily so...". In the Santa Rosa mylonite zone, phyllonites are, by Sibson's (1977) classification, a variety of ultramylonite; that is, they contain 90–100% matrix. Samples were classified as ultramylonite or phyllonite based on appearance in the field. Ultramylonite in the Santa Rosa mylonite zone is typically dark grey–black, largely aphanitic, and massive. A foliation is macroscopically visible, but the rock does not cleave easily. In contrast, phyllonite breaks easily along foliation planes (much like a slate), is generally grey–brown grey, and though the rock is dominantly aphanitic, a micaceous sheen is evident along foliation planes. Surprisingly, there is no microscopically evident explanation for the difference in macroscopic appearance between ultramylonite and phyllonite. They are compositionally, mineralogically and texturally similar. For the remainder of this paper, observations made from

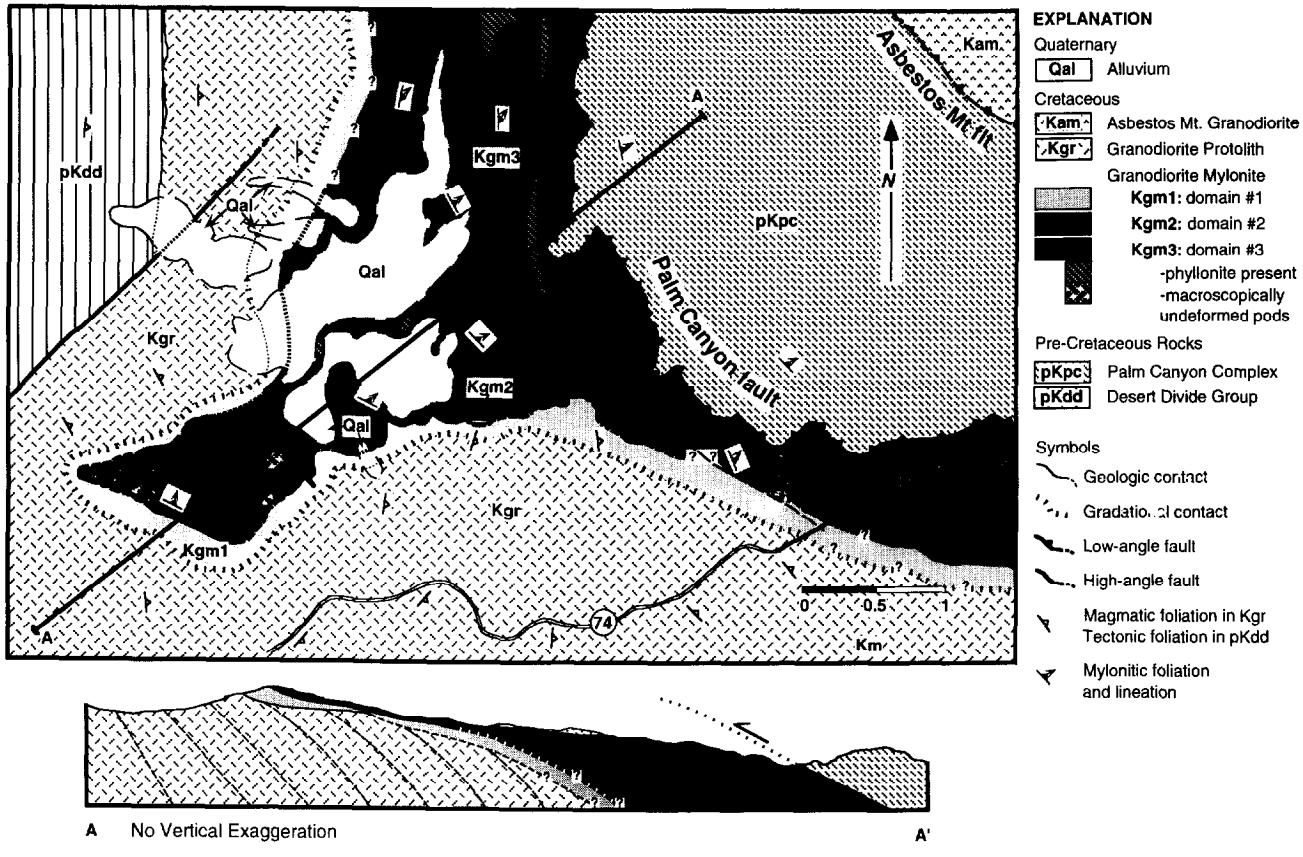

Fig. 2. Geologic map modified from that of Erskine (1985) shows distribution of the three structural domains described in the text. Unpublished mapping by L. Simmons, P. Jordan, K. Rich and Z. Zhong was used in the preparation of the map. Cross-section shows relations between the three structural domains. Dashed lines in granodiorite outside the mylonite zone schematically illustrate the trace of magmatic foliation. Sense of movement in the system is shown by arrow. Subsurface contacts constrained by field observations and structure contouring.

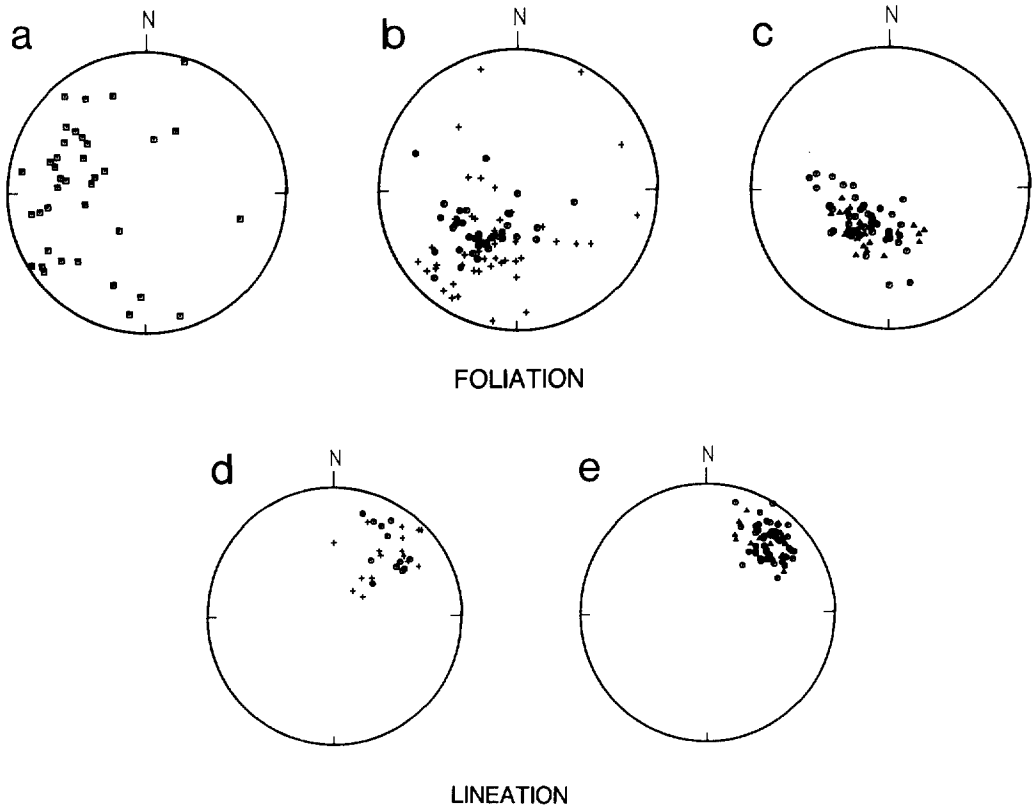

Fig. 3. Lower-hemisphere, equal-area projections. (a) Poles to magmatic foliation in granodiorite protolith. (b) Early stages of mylonitization: poles to micro-shear zone boundaries (crosses) and foliation in protomylonite and mylonite (circles), domain 1. (c) Late stages of mylonitization: poles to foliation in mylonite (circles), domain 3, and ultramylonite (triangles), domains 2 and 3. (d) Early stages of mylonitization: lineation in micro-shear zones (crosses) and protomylonite and mylonite (circles), domain 1. (e) Late stages of mylonitization: lineation in mylonite (circles), domain 3, and ultramylonite (triangles), domains 2 and 3.

the two rock types will be grouped together under the term 'phyllonite', which is dominant in the Santa Rosa mylonite zone.

Three foliations have been recognized in the Santa Rosa mylonite zone (Simpson 1984, Erskine 1985, O'Brien 1985, O'Brien *et al.* 1987). Fabric development is correlated with strain in the rock (Simpson 1984). *S*-surfaces (cf. Berthé *et al.* 1979) are dominant at low strains. Within highly strained phyllonite, *S*- and *C*-surfaces (cf. Berthé *et al.* 1979) are virtually parallel and shear bands (cf. White *et al.* 1980, Gapais & White 1982; extensional crenulation cleavages of Platt 1979, Platt & Vissers 1980; *C'* foliation of Ponce de Leon & Choukroune 1980) are pervasive. The composite *S–C* surface is the dominant, macroscopically visible foliation in the phyllonite.

Orientations of structures

The orientations of structures within the map area are shown in Fig. 3. Poles to the magmatic foliation (cf. Paterson *et al.* 1989) of the granodiorite protolith are shown in Fig. 3(a) and attitudes of *C*-surfaces in variably deformed rock from the mylonite zone are plotted in Figs. 3(b) & (c). These plots include data from the northernmost part of the Santa Rosa mylonite zone in addition to data from the main study area. Lineations, measured on *C*-surfaces of variably deformed rock from the mylonite zone, are shown in Figs. 3(d) & (e). The slight spread in orientation of poles to foliation visible in Figs. 3(b) & (c) lies in a plane at right angles to the lineations as a result of the gentle folding of the mylonite zone mentioned earlier. These plots illustrate two important points. First, the orientation of the magmatic foliation of the granodiorite protolith is distinct from the orientation of the tectonic foliations, supporting the assertion that mylonitization post-dated cooling of the granodiorite protolith. Second, the maxima defined by the *C*-surfaces and the lineations are stronger for more highly strained rocks, indicating that the orientations of these fabric elements became more regular with increasing deformation, from micro-shear zones and protomylonite, to mylonite, to phyllonite.

Bulk chemistry and mineralogy

Previous studies (Erskine 1985, O'Brien *et al.* 1987) show no systematic bulk chemical changes with increase in strain in the Santa Rosa mylonite zone. Our results are reported with respect to the percent matrix material developed through deformation, determined through petrographic analysis of the samples analyzed (Fig. 4). Although variation in the chemical constituents of different samples is apparent, it is not linked to degree of deformation. Such differences can be accounted for by heterogeneities in the granodiorite protolith which are

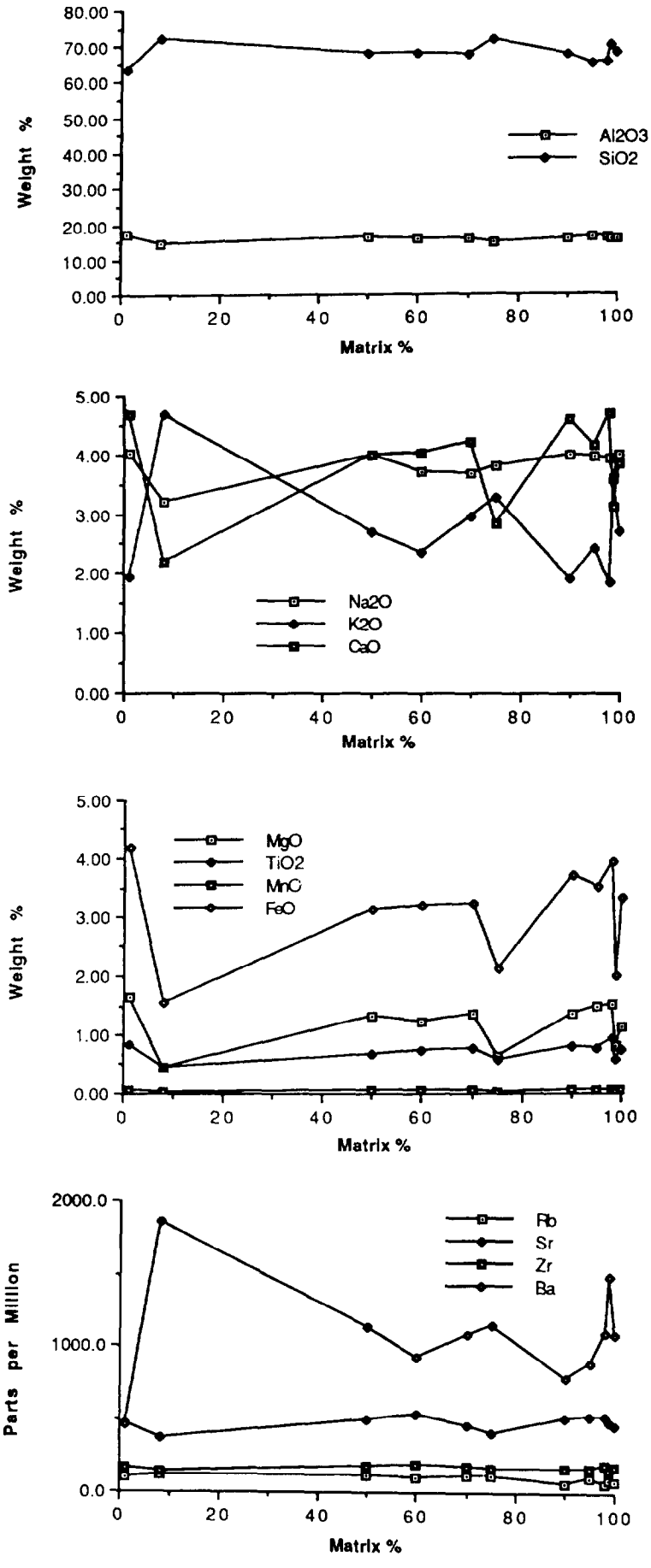

Fig. 4. Major, minor, and trace element analyses plotted as weight percent oxides or parts per million with respect to matrix percent; strain is not accompanied by consistent changes in composition. Note that the scale of the vertical axis varies from plot to plot.

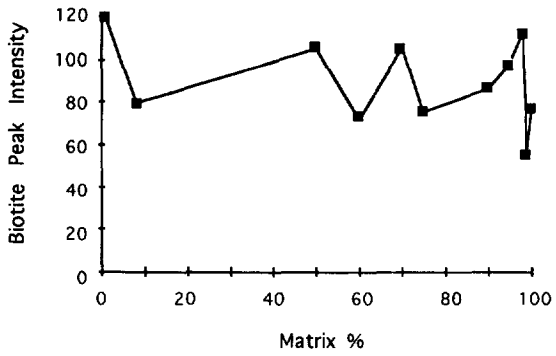

Fig. 5. X-ray diffraction data from samples analyzed for Fig. 4. Biotite peak intensity (measured in counts per second) is plotted against matrix percent. Variation in the amount of biotite correlates with composition (compare with Fig. 4), not with strain.

not erased by mylonitization. X-ray diffraction of whole-rock powders was used to investigate modification of bulk mineralogy during deformation. Two results of importance emerge: (1) biotite, the only hydrous phase present, changes in quantity with variation in bulk composition, but not with variation in amount of strain (Fig. 5, compare with Fig. 4). This observation contrasts sharply with O'Hara's (1988) study of phyllonite development in North Carolina, where deformation was accompanied by breakdown of alkali feldspar to form muscovite. (2) The only systematic change with deformation is shown by plagioclase feldspar. Plagioclase composition is $\sim An_{40}$ for the granodiorite protolith and An_{30-35} for mylonite (Ague 1988). Within the mylonite, the compositions of plagioclase porphyroclasts and subgrains within porphyroclasts are the same within measurement error (Ague 1988). Interestingly, the recrystallized 'tails' of plagioclase porphyroclast systems are slightly but consistently more calcic. Petrographic investigations suggest that accessory epidote formed during deformation; epidote probably accommodated Ca and Al released as plagioclase, overall, became more sodic.

In summary, fabrics within the Santa Rosa mylonite zone become increasingly well developed with increasing strain, but deformation is not accompanied by changes in bulk chemistry or mineralogy. In the following sections, we explore the structural changes that do accompany this strain increase, progressing from the granodiorite protolith structurally upward through the mylonite zone toward the Palm Canyon fault.

Granodiorite protolith

The plutonic protolith to the mylonite in the Santa Rosa mylonite zone is macroscopically heterogeneous. Within the study area it is predominantly granodiorite, although local variation from granite to granodiorite is evident in the field and more mafic microgranitoid enclaves (or autoliths, cf. Vernon 1984, Vernon *et al.* 1988) and schlieren are locally abundant. The rock is typically an equigranular, medium-grained granodiorite, but it is locally fine- or coarse-grained and, rarely, porphyritic. The major mineral constituents are, in order of abundance, plagioclase, quartz, biotite and potassium feldspar.

This granodiorite protolith exhibits a weakly to moderately developed, generally northerly striking and steeply E-dipping magmatic foliation (Figs. 2, 3a and 6a). The foliation is defined by the alignment of flattened microgranitoid enclaves and dimensional preferred orientation of subhedral biotite and feldspar phenocrysts (Figs. 6a & b). Inclusions vary in size and may reach several meters in longest dimension. They are generally lens-shaped and flattened in the plane of the foliation, but may be irregular in shape. In the area of study, the granodiorite protolith is not lineated.

Within the granodiorite protolith, undulatory extinction, occasional subgrain formation and some elongation of quartz grains are the only common signs of ductile deformation visible with the light microscope (Fig. 6b). Transmission electron microscope (TEM) analysis of microstructures in plagioclase—including exsolution lamellae, dislocation arrays, and subgrain walls—suggests that deformation occurred at a minimum temperature of 500°C (Ague 1988). Biotite is rarely kinked, is generally subhedral, and is characterized by straight grain boundaries. Features indicative of intracrystalline deformation in biotite are concentrated along these grain boundaries (Goodwin & Wenk 1990). These features consist of regions of intracrystalline folding and cataclasis, which are characterized by little or no change in color with rotation of the microscope stage and, in most orientations, higher refractive indices than the undeformed portions of the grains.

Domain 1: evidence for initial cataclasis and subsequent mylonitization

The boundaries of the mylonite zone are curviplanar (Fig. 2). Where good control is possible through structure contouring, the lower boundary is roughly parallel to the Palm Canyon fault. At the map scale, the magmatic foliation in the granodiorite protolith curves toward the base of the mylonite zone in a sense consistent with top-to-the-southwest displacement (Fig. 2). At the outcrop scale, the contact between the granodiorite protolith and structural domain 1 is irregular. This contact is broadly gradational, as shown on the map in Fig. 2, but strain does not increase continuously structurally upward; deformation was heterogeneous.

Domain 1 comprises the least deformed section of the Santa Rosa mylonite zone. Within this 15–75 m thick domain, the granodiorite protolith is cross-cut by 1–20 mm wide branching shear zones, which locally truncate the magmatic foliation and divide the granodiorite into lens-shaped pods (Fig. 6c; geometry reminiscent of Simpson 1982). Three types of micro-shear zone have been recognized: (1) the most common type appears to contain ultramylonite with a single macroscopically visible foliation, parallel to the micro-shear zone boundaries, and a mylonitic lineation. The mylonitic foliation and lineation are defined by the preferred crystallographic orientation of biotite, dimensional alignment of

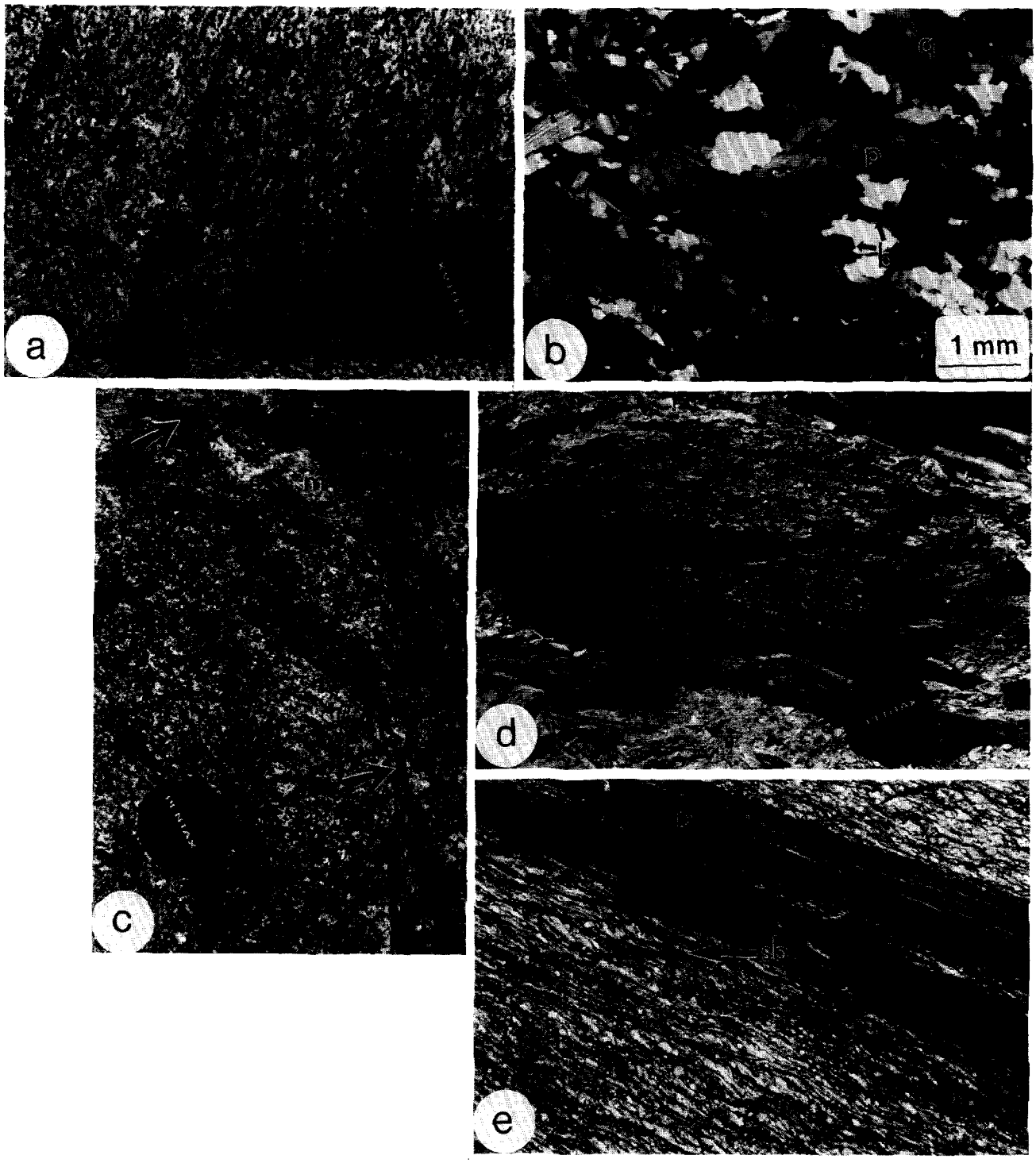

Fig. 6. (a) Granodiorite protolith; magmatic foliation defined by preferred dimensional alignment of biotite (black) and flattened microgranitoid enclaves (e). (b) Granodiorite protolith; trace of magmatic foliation, defined by preferred dimensional alignment of subhedral biotite grains (b) and plagioclase laths (p), is approximately parallel to the base of the photo. Undulatory extinction in quartz (q) is common. Thin section cut at right angles to foliation; polarizers crossed. (c) Domain 1; anastamosing micro-shear zones (marked by arrows) cross-cut granodiorite. 'm' indicates area of incipient mylonitization. (d) Domain 1; folded micro-shear zones. Black line traces the boundary between a micro-shear zone (left) and protomylonite (right), defining the fold. (e) Domain 3; note the sharp boundaries between the mylonite and the thin, laterally discontinuous phyllonite (p). The boundaries are parallel to *C*-surfaces. Shear bands (sb) indicate sinistral (top-to-the-southwest) displacement. The chisel is 15 cm long.

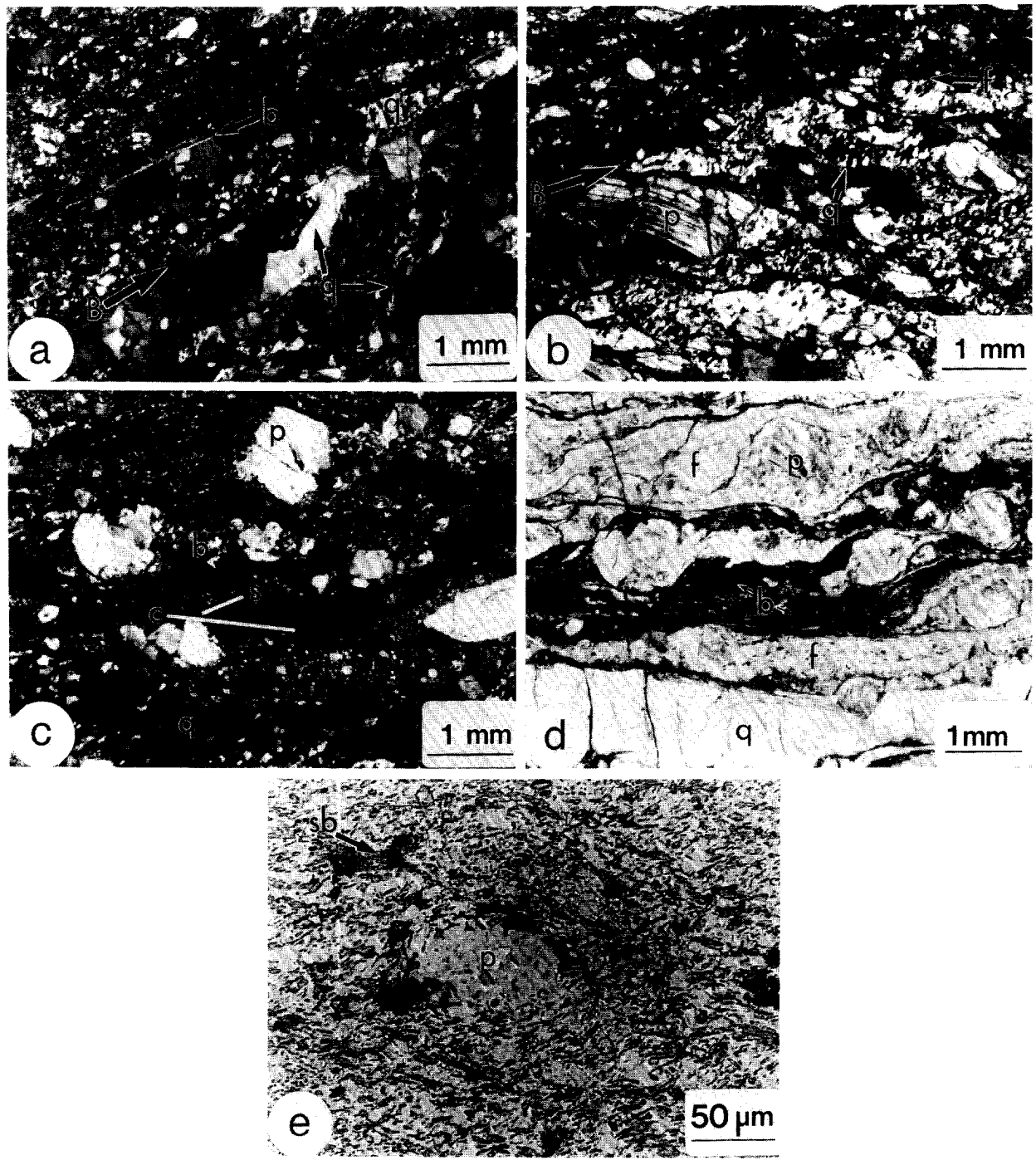

Fig. 7. Thin sections viewed at right angles to foliation and parallel to lineation. Polarizers are crossed in (a), (b) & (c). Sense of shear in (b)–(e) is dextral, or top-to-the-southwest. Domain 1: (a) 'B' marks boundary between micro-shear zone and macroscopically undeformed granodiorite. Biotite grains are locally strongly aligned (b) within the micro-shear zone. Quartz (q) exhibits undulatory extinction and, locally, ribbons. Both undulatory extinction and fractures are common in feldspars. (b) Ductile overprint of a micro-shear zone and the adjacent rock (now a protomylonite). Note sharp boundaries of micro-shear zone (B) and associated fractures (f). Plagioclase porphyroclasts (p) are fractured and bent. Long axes of quartz subgrains and new grains (q) define *S*-surfaces. Domain 3: (c) porphyroclast systems of feldspar (p) and biotite (b) in mylonite; orientations of *S*- and *C*-surfaces marked. Recrystallized quartz grains (q) are elongate parallel to *S*-surfaces. Feldspar porphyroclasts develop a rounded appearance and exhibit fewer fractures with decreasing grain size. (d) 'p' marks the plagioclase porphyroclast labeled in (c). f-domains are dominantly fine-grained feldspar, b-domains are mainly biotite, and q-domains are formed of fine-grained quartz. Domain 2: (e) ultra-thin section of phyllonite. Trace of *C*-surface is horizontal; 'sb' is shear band foliation; 'p' is rounded feldspar porphyroclast. Medium grey, rectangular grains concentrated along the shear band foliation are biotite. Note that grains lying along shear bands are no smaller than those in the surrounding rock.

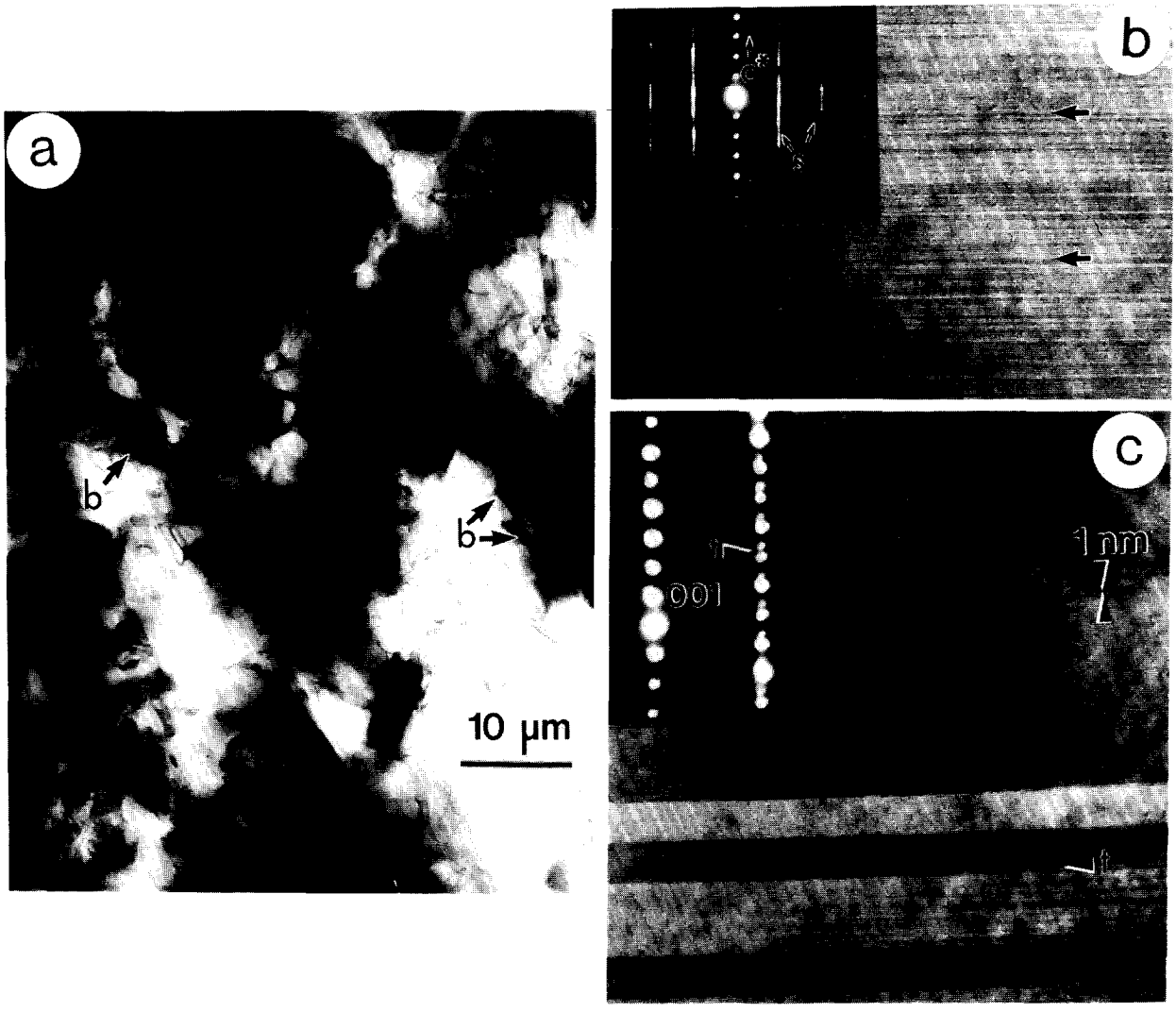

Fig. 8. (a) High voltage electron micrograph of ultramylonite sample PC-93, viewed at right angles to lineation and foliation. Biotite grains are imaged as platelets. Note straight grain boundaries. Main foliation trends roughly west-northwest. (b) & (c) lattice images of biotite grains in ultramylonite sample PC-93a. Two orientations are shown (see text for further explanation). (b) Representative stacking faults indicated by arrows. Spacing between lattice fringes is 1 nm. Note streaking in the diffraction pattern(s). (c) Diffraction pattern is enlarged to show doubling of reciprocal lattice points. Doubled points, (t), are caused by twinning. Twins (t) are imaged as broad bands of varying contrast, within which the finer 1 nm lattice fringes are visible.

quartz-rich domains and the direction of extension of fractured feldspar porphyroclasts. At least one boundary of a given micro-shear zone is usually sharp; at the other a mylonitic or magmatic foliation may curve towards the margin. (b) The thinnest micro-shear zones often have structureless interiors, composed of grey or black aphanitic, unfoliated material. Slickenside striae may be visible along the margins. This type generally exhibits very sharp borders that truncate the magmatic foliation in the granodiorite protolith. (c) The third, rare variety of micro-shear zone is an apparently continuous ductile shear zone (cf. Ramsay & Graham 1970, Ramsay 1980); this type is usually less than a few millimeters wide. Where the sense of displacement along micro-shear zones has been determined, it is top-to-the-southwest, consistent with other sense-of-shear indicators throughout the Santa Rosa mylonite zone. The orientations of micro-shear zones, and foliations and lineations within micro-shear zones, are shown in Fig. 3.

With the light microscope, the first two types of micro-shear zone exhibit sharp boundaries along which quartz and other minerals are abruptly truncated (Fig. 7a). Angular fragments of granodiorite, quartz and feldspars are often visible within the shear zones. The grain size of biotite within the bands is substantially reduced, so that individual grains are generally indistinguishable. These relations suggest cataclasis (microfracturing, movement along fractures, frictional grain-boundary sliding, and fragment rotation; cf. Paterson 1979, Knipe 1989). There is, however, some evidence for microscopically ductile deformation. Undulatory extinction in quartz is common, appearing locally to have preceded, but in most instances to have post-dated, cataclasis. This ductile overprint is more pronounced at structurally higher levels as the ultramylonite domain is approached. As deformation continues the material within the micro-shear zones develops into phyllonite, but the sharp boundary(ies) are maintained (compare Figs. 7a & b). These characteristics are reminiscent of shear zones developed experimentally through ductile deformation of pre-faulted aplite (Tullis *et al.* 1990).

Within domain 1, the spatial density of micro-shear zones increases and the pods of granodiorite protolith between the micro-shear zones generally become progressively more deformed structurally upward. Some micro-shear zones were folded during subsequent mylonitization (Fig. 6d), with fold axes parallel to the mylonite lineation. This structurally upward increase in deformation is not continuous, and macroscopically undeformed pods may be found in contact with the second structural domain. In general, however, macroscopically undeformed rock is more common at lower structural levels and mylonitized rock is dominant as the contact with domain 2 is approached.

Deformation within pods between micro-shear zones in domain 1 did *not* involve initial whole-rock cataclasis (Figs. 6c and 7b); instead, progressive reduction in grain size took place by mechanisms that varied from mineral to mineral. Observations of variably deformed rock within domain 1 indicate that mylonitization in these pods initiated with subgrain development during formation of quartz ribbons. Plagioclase deformed by fracturing and dislocation glide, and recrystallization was driven by high dislocation densities (Ague 1988); undulose extinction is also common in feldspars. Zones of intracrystalline deformation in biotite became more extensive, extending into the grains from grain margins and resulting in an abrupt decrease in biotite grain size (Goodwin & Wenk 1990). During this deformation, mineralogical domains, visible in hand specimen and with the light microscope, developed. Minerals are segregated within these domains as follows: (1) quartz, (2) quartz and feldspar, (3) feldspar, (4) quartz, feldspar and biotite, and (5) biotite, locally with accessory amphibole, epidote and titanite.

S- and *C*-surfaces were present at all stages of the deformation, developing simultaneously (Fig. 7b). *S*-surfaces are defined by the dimensional preferred orientation of quartz grains within quartz domains and by the long dimensions of biotite porphyroclasts. *C*-surfaces are parallel to the boundaries of mineralogical domains. As deformation progressed, the spacing between mineralogical domains became smaller, the number and size of porphyroclasts decreased, and *C*-surfaces became increasingly dominant over *S*-surfaces (compare Figs. 7b–e). The *S*-surfaces rotated toward the *C*-surfaces with increasing deformation. This sequence of development of mylonite and mylonitic fabrics from granodiorite protolith is also recorded by protomylonite and mylonite in domain 3.

Domain 2: phyllonite dominant

The contact between the first and second structural domains is typically sharp. Both the micro-shear zones and relict magmatic foliation within domain 1 are bent into the base of domain 2, indicating that the foliation in domain 2 is the youngest structure. The sense of displacement recorded by this deflection of older structures is, again, top-to-the-southwest. Domain 2 is predominantly phyllonite, locally including lenses and layers of protomylonite and mylonite. A single, regular, very well developed foliation and lineation is visible in the field (Fig. 3). The outcrop pattern of domain 2 has been simplified for Fig. 2; in the field it is seen to vary and to branch, in places forming discontinuous lenses or folds.

The 3–12 m thick domain 2 is essentially continuous within the area indicated in Fig. 2. It has also been observed in a traverse across the northernmost part of the mylonite zone, just southwest of Palm Springs (refer to Fig. 1). Between the latter area and the questioned portion of the domain in Fig. 2 its existence has not been verified, but it appears probable that it continues throughout the mylonite zone.

Petrographic observations indicate that feldspar porphyroclasts in the phyllonite have rounded profiles and are generally *not* fractured (Fig. 7e); biotite porphyroclasts are absent. Fractures generally are not observed in smaller feldspar porphyroclasts in mylonitized rocks throughout the zone, suggesting that the deformation

mechanisms in feldspars varied with grain size. Grain boundaries of all minerals in the phyllonite are generally straight and quartz and feldspar grains in the matrix are typically equant, suggesting recovery. Biotite seldom shows obvious signs of deformation (see later sections); typically, a few grains are gently bent.

Quartz-rich mineralogical domains are locally present in phyllonite, parallel to *C*-surfaces, and decrease in number and thickness as porphyroclasts decrease in number and size. This general homogenization of the fabric of the rock is characteristic of phyllonite within the Santa Rosa mylonite zone. Where present, mineralogical domains may be folded, with fold axes parallel to the mylonitic lineation and axial planes parallel to the dominant composite *S–C* foliation. Macroscopic folds, sometimes in the layers and lenses of protomylonite and mylonite mentioned above, are also evident in domain 2. These folds are similar in appearance to folds developed within domain 1 (Fig. 6d). In addition to the composite *S–C* foliation, which is visible in outcrop, a well-developed shear band foliation is typical of the phyllonite (Fig. 7e). Biotite appears to be concentrated along the shear band foliation planes. Although evidence for early cataclasis has not been preserved in domain 2, the typically sharp boundaries to the domain, its locally branching character, and the presence of macroscopic folds in and within the domain all suggest that phyllonite in domain 2 had an origin similar to phyllonite in domain 1.

Domain 3: mylonite domain

The contact between domains 2 and 3 may be sharp or may consist of phyllonite and mylonite intermixed over a third of a meter to a meter interval. Domain 3 comprises the bulk of the mylonite zone and is predominantly mylonite with minor amounts of protomylonite, thin (~1–50 cm thick), laterally discontinuous phyllonite (Fig. 6e) and rare macroscopically undeformed pods which are sometimes bounded by phyllonite. Mappable undeformed pods and areas where phyllonite is relatively common have been delineated within domain 3 (Fig. 2). We have certainly not mapped all of these heterogeneities, but our current map illustrates that they are widely distributed. The undeformed pods range in size from roughly 2–200 m in longest dimension. They are typically more mafic than the surrounding rock, suggesting that more mafic plutonic material is rheologically more competent. The local presence of essentially undeformed pods, or lenses of anomalously low strain, within the main part of the mylonite zone may therefore reflect compositional heterogeneities inherited from the protolith. Compositional variations are retained in the mylonite in other ways as well. Folds in compositionally distinct layers are common, and small microgranitoid enclaves are still recognizable despite deformation.

C-surfaces, *S*-surfaces and shear band foliations (Figs. 6e, 7c & d) indicate top-to-the-west displacement, as noted by previous workers (Erskine 1985, Simpson 1984). Development of mylonite and foliations in mylonite occurred as described for deformation of pods between micro-shear zones in domain 1. Phyllonite layers and lenses are either parallel to or inclined at a small angle to the *C*-surfaces. At least one contact between a given phyllonite zone and the surrounding mylonite is typically sharp (Fig. 6e). Locally, thin (cm-scale) zones of phyllonite exhibit gradational contacts with the surrounding mylonite.

Within the map area, the mylonite domain is truncated by the Palm Canyon fault, which dips gently to the northeast and separates the mylonitic plutonic rocks from the overlying mylonitized metasedimentary rocks of the Palm Canyon Complex (Fig. 2). To the north, the fault ramps upward from the contact between the granodiorite and metasedimentary mylonites, which is demonstrably a modified intrusive contact, suggesting that displacement along the fault was modest. Beneath the Palm Canyon fault, the mylonite is brecciated and strongly chloritized. Minerals in fractures within the fault zone include calcite, laumontite and prehnite. The fault therefore is a brittle, post-mylonitic feature. Mylonitization and subsequent faulting took place during cooling of the batholith, and emplacement of the uppermost thrust sheets occurred at *ca.* 200°C (Goodwin & Renne 1991).

DEVELOPMENT OF FABRIC WITH INCREASING STRAIN

Regions of phyllonite mark zones of high strain in all three structural domains within the heterogeneously deformed Santa Rosa mylonite zone. We have demonstrated that phyllonite developed through ductile overprinting of cataclastic micro-shear zones in domain 1. It forms the bulk of domain 2 and is locally developed in domain 3. In total, phyllonite composes approximately 5% of the mylonite zone.

Petrographic observations indicate that reduction in grain size occurs in two very different ways within the Santa Rosa mylonite zone. The first involves an initial abrupt decrease in grain size through cataclasis, followed by ductile deformation. Where it can be shown that phyllonite was produced in this way, following initial cataclasis in domain 1, it is characterized by sharp contacts with the surrounding rock. In domains 2 and 3, sharp boundaries are also typical of phyllonite (e.g. Figs. 6d & e, 7a & b), suggesting that phyllonite formed everywhere through ductile flow following initial cataclasis. The second way involves a progressive, rather than abrupt, reduction in grain size *outside* micro-shear zones by mechanisms that vary from mineral to mineral. As the grain size is reduced, the rock passes through the stages of protomylonite (10–50% matrix) and mylonite (50–90% matrix), which cannot happen if there is initial cataclasis (90–100% matrix observed in micro-shear zones in the Santa Rosa mylonite zone). Protomylonite and mylonite, which compose ~94% of the mylonite zone, therefore can only be produced through this progressive reduction in grain size.

In a continuous ductile shear zone (cf. Burg & Laurent 1978), the boundaries between high-strain and low-strain regions of the shear zone are gradational (i.e. Ramsay & Graham 1970, Ramsay 1980), but gradational boundaries are rarely observed in the Santa Rosa mylonite zone. Sharp boundaries, or discontinuities, are produced in this case through initial whole-rock cataclasis followed by ductile flow.

As noted earlier, foliations in phyllonite of the Santa Rosa mylonite zone are distinctive. This point is further explored in the following sections, in which we present X-ray texture, TEM and high voltage electron microscope (HVEM) studies of biotite, the main foliation-forming phase.

DEFORMATION OF BIOTITE IN PHYLLONITE

Experimental procedures

Hand samples were cut and thin sections were made at right angles to *C*-surfaces, and both parallel and perpendicular to a mineral lineation. TEM mounts made from these thin sections were therefore oriented with respect to macroscopic fabric coordinates, allowing features seen with the electron microscope to be correlated with field and petrographic relations. As biotite is the main foliation-forming mineral, biotite basal planes are oriented at a high angle to these TEM mounts. The (001) planes were therefore subnormal to the specimen section. TEM mounts of biotite were prepared by ion or atom bombardment, through which thin holes in the sample section were produced for viewing. The correlation between electron microscope and petrographic or field observations is simplified by the generation of HVEM 'maps' of holes of interest. The 1500 kV acceleration of the Kratos HVEM (National Center for Electron Microscopy, Lawrence Berkeley Labs, California) provides more than five times the sample penetration of a standard 100 kV TEM. This allows one to work at very low magnifications—in this case 1000X magnification—and photograph relatively large areas. An enlargement of an HVEM photomicrograph is shown in Fig. 8(a) (compare with Fig. 7e). Biotite grains show strong contrast when they are oriented with (001) parallel to the electron beam.

A 100 kV Siemens 102, equipped with a LaB_6 filament, was used for lattice imaging. The study was facilitated by a top-entry, ±45° double-tilt stage. All data were obtained viewing basal planes edge-on, i.e. with the electron beam parallel to (001). Phase contrast analysis was used for lattice imaging. An objective aperture was placed symmetrically about the transmitted beam to include (005) reflections.

TEM and HVEM observations

In general, biotite is distributed fairly evenly throughout regions of phyllonite (Fig. 7e). HVEM images (Fig. 8a) indicate that larger biotite grains are often clustered; clusters are typically randomly distributed throughout the rock and are laterally discontinuous within the planes studied. The concentration of biotite grains along foliation surfaces, visible at a larger scale (Simpson 1985, O'Brien *et al.* 1987; Fig. 7e), is only locally evident within the thicker regions of some TEM foils. Petrographic study of sample mounts, however, indicates that they encompass multiple *S–C* surfaces and shear bands. Biotite from all foliation surfaces exhibits similar features. In contrast to protomylonite and mylonite, in which intracrystalline folding and cataclasis of biotite is a major deformation mechanism (Goodwin & Wenk 1990) and biotite 'fish' are common, biotite in phyllonite shows features which, cumulatively, suggest dynamic recrystallization. These include: (1) straight grain boundaries and sub- to euhedral grain shapes, (2) virtually no bending or kinking of grains and no intracrystalline folding and cataclasis, (3) high densities of randomly spaced stacking faults, which are present only near regions of intracrystalline deformation in biotite from protomylonite and mylonite (Goodwin & Wenk 1990), (4) small but consistent changes in the composition of biotite accompanying deformation, and (5) elongation of biotite grains parallel to lineation. These observations are not consistent with cataclasis, and therefore record the modification of biotite microstructures during ductile flow subsequent to cataclasis. While at least some of these features might be attributable to post-deformation annealing, there are two lines of evidence that suggest that this is not the case. First, it is difficult to see how either the average grain size of biotite in phyllonite—on the order of 5 μm—or biotite's elongation parallel to the lineation could be maintained through annealing. Second, the record of cooling during deformation in the Santa Rosa mylonite zone (Goodwin & Renne 1991) is inconsistent with a re-heating event. We enlarge on these points in the following sections.

Microprobe analyses of biotite document small but consistent compositional changes (a decrease in Ti and Ba and an increase in Ca) that accompany deformation, suggesting that biotite is recrystallizing as deformation progresses (Goodwin & Renne 1991). Recrystallization is consistent with the straight grain margins and rectangular shapes of biotite imaged by HVEM (Fig. 8a), the fact that only 5–6% of the grains investigated were bent or kinked, and the absence of evidence for intracrystalline folding and cataclasis—none of which are consistent with initial cataclasis. A comparison of TEM observations of biotite in phyllonite with TEM observations of biotite in mylonite (Goodwin & Wenk 1990) is also informative. Typical grains in both mylonite and phyllonite exhibit 1 nm lattice fringes (Figs. 8b & c), indicative of the most common, 1M, polytype of biotite (cf. Smith & Yoder 1956). Irregularly spaced stacking faults (planar defects across which the order of the crystal changes) are spatially associated with regions of intracrystalline folding and cataclasis in biotite porphyroclasts in mylonite, suggesting that intracrystalline slip accompanied folding and cataclasis (Goodwin & Wenk 1990). In contrast, high densities of irregularly spaced stacking faults are ubiquitous in biotite in phyllonite and produce

streaking in diffraction patterns (Fig. 8b). While a diffraction pattern is typically designated by the zone axis parallel to the electron beam (e.g. a $0k\ell$, $hh\ell$, or $\bar{h}h\ell$ reciprocal lattice net, following Bell & Wilson 1977), streaking is often so extensive in biotite in phyllonite that such a designation is not possible. In effect, the irregularly spaced stacking faults have resulted in randomly superimposed reciprocal lattice nets. There is no evidence for intracrystalline folding and cataclasis.

Twins are developed only adjacent to regions of cataclasis in biotite porphyroclasts in mylonite, but are common in biotite in phyllonite. Twins are imaged as contrasting stripes, and are recorded by the doubling of reciprocal lattice points (Fig. 8c). The diffraction pattern in Fig. 8(c) is an $h0\ell$, $h3h\ell$, or $\bar{h}3h\ell$ net; twins may be either [110] axis, rotated $-60°$ about c^*, or [100] axis, rotated 180° about c^*. Twins and stacking faults may be growth features, and/or may be related to intracrystalline slip.

Preferred orientation of (001): pole figures

The orientations of (001) planes of biotite in phyllonite were measured with an X-ray texture goniometer in transmission geometry using the method and data processing procedures described by O'Brien (1985). The results (Fig. 9a) are consistent with those of O'Brien *et al.* (1987). Pole figures show a strong preferred orientation of (001) planes, with a single asymmetric peak. Biotite flakes are, on average, inclined slightly toward the down-dip direction of the lineation, out of the plane of the composite *S–C* foliation. In sections at right angles to the lineation, biotite flakes exhibit a wide range of tilting with respect to the *S–C* foliation.

The (001) pole figures of phyllosilicates may be used as sense-of-shear indicators (O'Brien *et al.* 1987), based on the premise that the pole figure asymmetry reflects the fabric asymmetry, as foliation planes are often defined by the preferred dimensional orientation of phyllosilicate grains. The (001) pole figures of biotite from the Santa Rosa mylonite zone exhibit a consistent sense of asymmetry with respect to macroscopic structures (Fig. 9a; O'Brien *et al.* 1987). The asymmetry of these pole figures reflects the distribution of the biotite grains between the *S–C* foliation and shear bands (Fig. 7e), and is consistent with top-to-the-southwest shear. Wenk & Pannetier (1990) observed that (110) + (020) pole figures from mylonite and phyllonite in the Santa Rosa mylonite zone have a maximum in the lineation direction. This could be due to an axial alignment within the basal plane (as the deconvolution of Helming *et al.* 1994 suggests) or simply due to the spread of (001) poles on a great circle normal to the foliation. If the former is true, an axial alignment would indicate intracrystalline slip. Kronenberg *et al.* (1990) report that experimentally deformed biotite is measurably weaker in directions [100] and [110] than in directions [010] and [310]. Dislocations are confined to the (001) plane, with Burgers vectors of 1/2<110> and <110> (Kronenberg *et al.* 1990, Christoffersen & Kronenberg 1993). If the latter applies then the orientation of biotite may be mainly due to the plate-like grain shape and grains may undergo rigid rotations. This is further investigated with HVEM observations in the following sections.

Preferred orientation of (001): trace analysis

Trace analysis of biotite grains in HVEM photomicrographs allows a more complete evaluation of (001) pole figures than is possible with petrographic observations. Very fine grains that are not visible with the optical microscope can be seen easily with the HVEM. The apparent length (l') and apparent thickness, or *c*-axis dimension, (t') of each grain is measured as shown in Fig. 9(b). The angle θ between l' and the trace of the *C*-surface (marked on each oriented TEM mount and transferred to each HVEM map) is also determined. While a single TEM mount is just 3 mm in diameter, we suggest that these measurements are nonetheless significant since HVEM photomicrographs of other samples of phyllonite exhibit similar features, there is an excellent correlation between trace analyses and (001) pole figures (Fig. 9; O'Brien *et al.* 1987), and the phyllonite is so fine-grained and homogeneous that this is a representative sample size. The error associated with petrographic measurements of l' and t' has been determined to be approximately ±5%, and 200 grains constitute a statistically representative sample (Jones & Galwey 1972); we assume a similar error applies to the measurements reported here.

Trace analyses of two sections through sample PC-93 are compared to its (001) pole figure in Fig. 9. Section A was cut parallel to lineation and normal to the *S–C* foliation and section B was cut at right angles to both the lineation and the *S–C* foliation. Traces of these sections are plotted on the pole figure. The mean plate diameter of biotite grains is 3 μm (in general, the grain size of biotite in phyllonite samples from the Santa Rosa mylonite zone is on the order of 5 μm). Histograms of the areas ($l' \times t'$ vs. θ) of different sizes of grains (Figs. 9c & d) illustrate several important points: (1) the distribution of the area of biotite grains with orientation reflects the symmetry of the pole figure (indicating that trace analyses have been made on a representative sample of grains), (2) although less numerous than the smaller grains, the larger grains have greater areas and therefore contribute greater intensities to the pole figure, (3) the larger grains have a stronger preferred orientation than the smaller grains, and (4) grains are, on average, longer parallel to the lineation (PC-93a; Fig. 9c) than at right angles to the lineation (PC-93b: Fig. 9d). Comparison between the histograms and pole figure also indicates that the error in θ is as much as ±15°; this represents the accumulation of errors in transferring an orientation mark from a rock sample, to a thin section, to a TEM grid, and finally to a photo collage. The observations emphasized here, however, are not compromised by this error.

Histograms showing the variation of aspect ratio (l'/t') with grain size indicate that aspect ratios increase

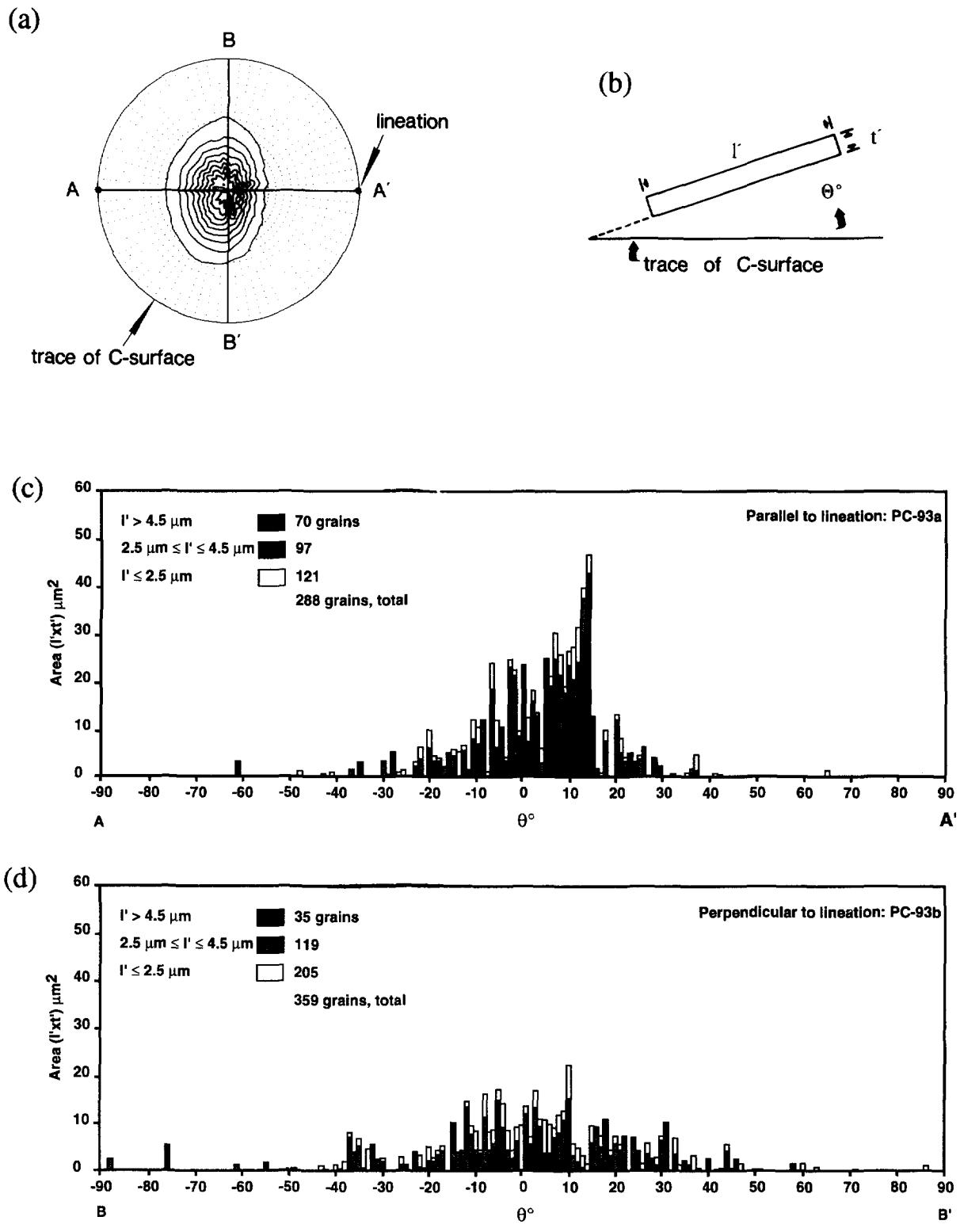

Fig. 9. Trace analyses of biotite in ultramylonite sample PC-93. (a) (001) pole figure, measured with an X-ray texture goniometer in transmission and plotted in lower hemisphere, equal-area projection. Intensities are contoured in multiples of random distribution; the lowest contour is 1.00, below which the figure is shaded; higher contours are 3, 5, 7, etc. Pole figure shows the position of sections A–A′ and B–B′ with respect to macroscopic fabric coordinates and the measured texture. Composite *S*–*C* foliation is parallel to the plane of the paper and the lineation lies within the plane of the foliation with the down-dip direction to the left. (b) Explanation of measurements of l', t' and θ are made. θ is negative for counterclockwise rotations, positive for clockwise rotations. (c) & (d) Histograms of areas of grains of different sizes with respect to θ determined from measurements along sections A–A′ and B–B′, respectively.

with increasing grain size (Fig. 10). Also, the smaller the grains, the smaller the variation in aspect ratios. As biotite grains increase in size, both the average aspect ratios and the variation in aspect ratios increase.

In summary, observations of biotite in phyllonite include: (1) biotite grains have a strong crystallographic (and, therefore, dimensional) preferred orientation; larger grains exhibit less variation in orientation than smaller grains. (2) Aspect ratios of grains of different sizes suggest that biotite grains are initially approxi-

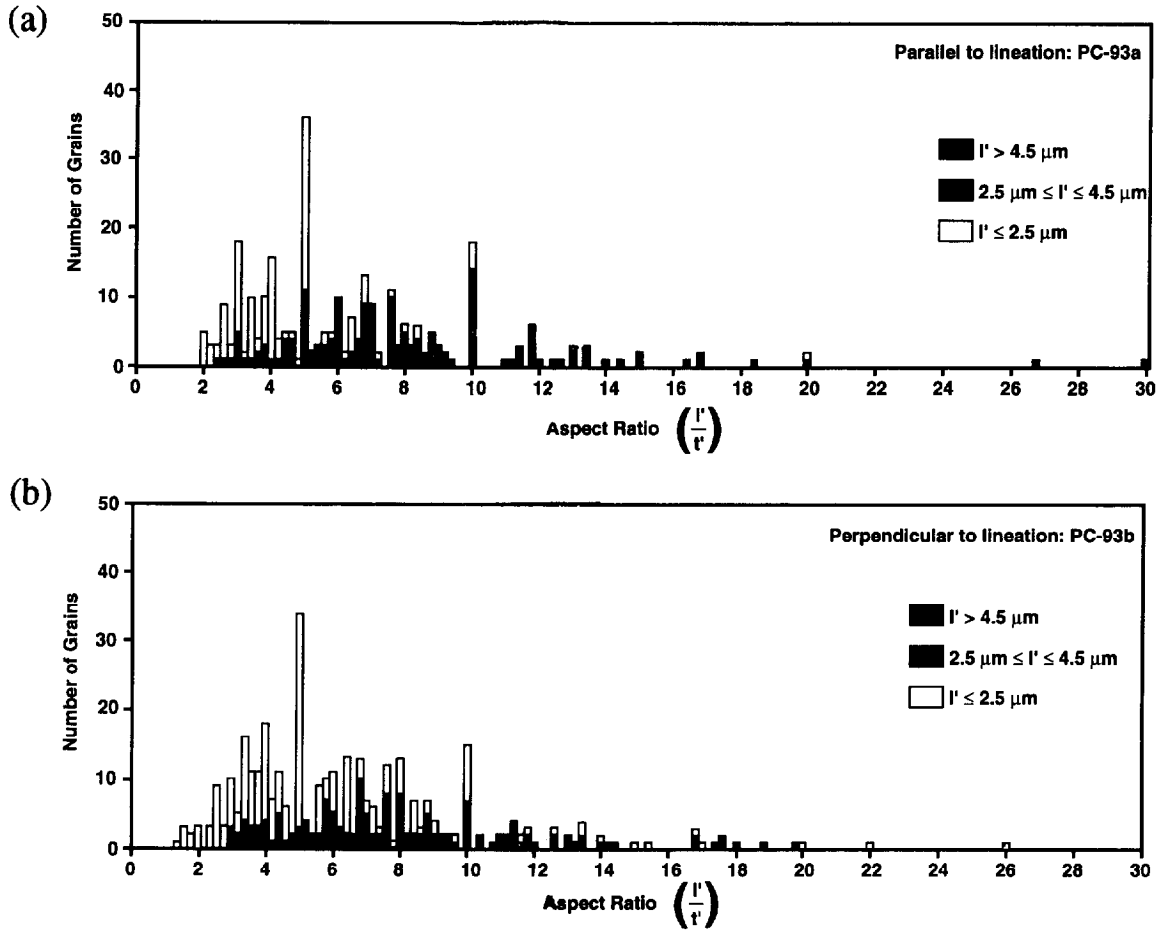

Fig. 10. Histograms of the same sections shown in Fig. 9, illustrating the number of grains of different sizes that have given aspect ratios. Note the similarity of the diagram parallel to lineation (PC-93a) and that at right angles to lineation (PC-93b).

mately the same size and shape in any section at right angles to the foliation. With increasing grain size, the aspect ratios increase; in other works, grain growth parallel to the basal planes is favored. (3) Biotite grains are elongate, and larger, in the direction of the lineation. If (110) poles are preferentially aligned parallel to the lineation (Helming *et al.* 1994), then grains are elongate parallel to [110]. (4) Biotite exhibits no bending, kinking, or intracrystalline folding and cataclasis, but stacking faults and twins are common. (5) Biotite exhibits straight grain boundaries and sub- to euhedral crystal shapes. (6) Small but consistent changes in composition of biotite accompanied deformation (Goodwin & Renne 1991). Large grains may be more strongly oriented than small grains because growth of biotite flakes that lie parallel to the *C*-surfaces is favored, because grains are rotating into the plane of the *C*-surfaces as they grow, or both. Some preferred orientation of even the smallest grains suggests that mechanical rotation probably accommodated some of the deformation. The presence of irregularly spaced stacking faults and twins, as well as the alignment of (110) poles parallel to lineation (Wenk & Pannetier 1990, Helming *et al.* 1994), suggests that intracrystalline slip is occurring. Collectively, these observations suggest that dynamic recrystallization, favoring growth of biotite grains parallel to the lineation, accommodated deformation in concert with intracrystalline slip and mechanical rotation.

DISCUSSION

An obvious question that arises from the observations reported here is: why would initial deformation in the Santa Rosa mylonite zone, which took place at a relatively high temperature, occur by localized cataclasis? We speculate that the rheologically strong granodiorite protolith was unable to accommodate regionally imposed stresses through macroscopically ductile flow throughout the Santa Rosa mylonite zone, and therefore failed along narrow zones of cataclasis. Cataclasite, formed within micro-shear zones and within areas that are now phyllonite, records deformation within zones much narrower than the present extent of the Santa Rosa mylonite zone. Cataclastic failure within such thin zones suggests higher strain rates than could be accommodated through ductile flow over a wider zone. Cataclasis therefore might allow a higher regional displacement rate than could be accomplished by macroscopically ductile flow, and/or could simply be the most efficient mechanism by which the zone could accommodate imposed stresses.

In addition to relieving stress, cataclastic failure created fine-grained regions that might be expected to be rheologically weaker than the granodiorite protolith. Not only was the grain size significantly reduced—the original rock fabric was destroyed, resulting in a more homogeneous distribution of phases in the rock. The more random distribution of phases could inhibit the growth to equilibrium grain size (Twiss 1977) of the individual mineral constituents, effectively stabilizing this fine grain size. Etheridge & Wilkie (1979) point out that very small, non-equilibrium grain sizes may be maintained during dynamic recrystallization in a multiphase rock, where the growth to equilibrium grain size of the mineral of interest is inhibited by another phase. A more random distribution of different phases will also accelerate strain because of the enhanced diffusivity between unlike phases (Etheridge & Wilkie 1979).

This grain-size reduction and stabilization was accompanied by development of a strong fabric that is distinct from that in the less deformed mylonite or protomylonite. In order to evaluate the potential influence of grain-size reduction on fabric development, previously documented evidence for deformation mechanisms operating in major minerals other than biotite should be considered. As indicated earlier, quartz and feldspar grains in phyllonite are typically equant, with straight grain boundaries. Crystallographic preferred orientations of plagioclase are weak in the granodiorite mylonite; however, they become stronger in the phyllonite (Wenk & Pannetier 1990). There is no evidence to suggest whether the development of a crystallographic preferred orientation in plagioclase at high strains occurred through recrystallization or intracrystalline slip. There is a strong crystallographic preferred orientation present in quartz in granodiorite mylonite from the Santa Rosa mylonite zone (Erskine & Wenk 1985, Wenk & Pannetier 1990). This preferred orientation is not present in phyllonite. This suggests that intracrystalline slip may be succeeded or dominated by mechanisms such as grain-boundary sliding once the grain size of quartz is reduced in phyllonite. Grain-boundary sliding may be accommodated by dislocation glide and climb throughout the deforming grains, through dislocation glide and climb along grain boundaries and within the grain mantle, or through grain-boundary diffusion (Gifkins 1976). The latter two accommodation mechanisms are not expected to result in good crystallographic preferred orientations. In fact, grain-boundary sliding generally results in little to no crystallographic preferred orientation (e.g. Boullier & Guegen 1975, Behrmann & Mainprice 1987) and grains are typically equant, rather than elongate parallel to fabric elements. In summary, there is good evidence that quartz is accommodating deformation dominantly through grain-boundary sliding, though other deformation mechanisms are dominant in biotite and plagioclase.

Phyllonite in the Santa Rosa mylonite zone developed a strong fabric distinct from that in less deformed mylonite or protomylonite. Specifically, *S*- and *C*-surfaces are virtually parallel and shear bands are pervasive at the microscopic scale in phyllonite (Fig. 7e). The former may be attributed to high strain; the latter is more unusual and less easily explained. It is interesting that the reduction in grain size along shear bands which has been described elsewhere (Gapais & White 1982) is absent in the Santa Rosa mylonite zone. As noted earlier, no alignment of biotite along specific foliation planes can be distinguished in the very thin samples examined with the electron microscope. Biotite in all areas of the samples examined exhibited similar microstructures, and showed the same trends as outlined by trace analyses. This leads us to suggest a link between the dominant deformation mechanisms and the character of the fabric that develops. In this case, the combination of dominant grain-boundary sliding in quartz, dynamic recrystallization and/or intracrystalline slip in plagioclase, and dynamic recrystallization in concert with intracrystalline slip and mechanical rotation of biotite may facilitate formation of small-scale shear bands, and accommodate strain within shear bands without further reduction in grain size.

SUMMARY AND CONCLUSIONS

Using the definition of Burg & Laurent (1978), the Santa Rosa mylonite zone is a discontinuous ductile shear zone: a continuous increase in shear strain from the shear zone boundary to its center (cf. Ramsay & Graham 1970, Ramsay 1980) is lacking. The consistent orientations of structures and the consistent sense-of-shear indicators recorded in all three structural domains suggest that all of the post-intrusion structures described herein developed during a single deformational episode. Strain was heterogeneous in space, as indicated by: (1) the presence of three distinct structural domains, (2) the position of the domain of highest strain near the lower boundary of the mylonite zone, and (3) the presence of macroscopically undeformed pods and phyllonite distributed irregularly throughout the first and third structural domains. Strain was also heterogeneous over time, as shown by the development of phyllonite following early cataclasis, as well as by the late stage brittle faulting. These observations are not surprising in that spatial and temporal heterogeneity is to be expected with flow in natural materials (Jiang 1994a,b, Jiang & White 1994).

Deformation in the Santa Rosa mylonite zone was isochemical and mineralogical changes during deformation were minor (plagioclase generally became more sodic and epidote developed as an accessory phase). Evidence for extensive fluid flow is absent. Reaction softening can therefore be eliminated as a possible mechanism for localizing strain within zones of phyllonite. Instead, micro-shear zones in which the grain size was reduced through whole-rock cataclasis served to localize subsequent ductile strain. Evidence of cataclasis is preserved in zones of phyllonite in the form of sharp boundaries with the surrounding rock, reminiscent of those produced experimentally through ductile flow

following faulting of aplite and albite rock (Tullis *et al.* 1990). Phyllonite therefore developed without the alteration of original mineral assemblages typically associated with retrogression—a process of formation that has not previously been documented, but is entirely consistent with the definition of phyllonite as stated by Sander (1911) and Knopf (1931).

Phyllonite development through ductile deformation of micro-shear zones was accompanied by ductile deformation of areas between the micro-shear zones. The bulk of the mylonite zone did not experience whole rock cataclasis. Deformation in these areas took place by a gradual reduction in grain size. Deformation within the Santa Rosa mylonite zone therefore occurred by two routes: (1) granodiorite → cataclasite → phyllonite; and (2) granodiorite → protomylonite → mylonite.

Biotite in phyllonite, with an average plate diameter of 3 μm, accommodated strain by dynamic recrystallization in concert with intracrystalline slip and mechanical rotation. Through these processes, a strong crystallographic preferred orientation is developed. The distinctive foliations in phyllonite of the Santa Rosa mylonite zone lead us to suggest that the character of foliations is linked to the main deformation mechanisms by which the mineral constituents of a rock accommodate strain.

Acknowledgements—L. B. Goodwin wishes to thank L. E. Weiss for thought-provoking discussion of the nature of deformation in shear zones; the National Center for Electron Microscopy at the Lawrence Berkeley Laboratory in Berkeley, California for providing access to the electron microscopes used in this study; D. M. Ague for numerous useful discussions; and field assistants S. Krueger and E. Zachgo for enthusiasm and energy. Support through NSF grants EAR-8416938, -8709378, and 9017237 to HRW; and Geological Society of America Award 3579-86, two Chancellor's patent fund grants from the University of California at Berkeley, and Phyl's Garage Fund to LBG is gratefully acknowledged. We thank the U.S. Forest Service for liberal use of campgrounds and Mike Dunn for providing access to private roads. Thoughtful reviews by J. C. White, S. Ralser, J. P. Evans and L. Dell'Angelo improved the text.

REFERENCES

Ague, D. M. 1988. Natural deformation of plagioclase: a microstructural investigation. Ph.D. Thesis, University of California at Berkeley, Berkeley, California.

Ague, J. J. & Brimhall, G. H. 1988. Magmatic arc asymmetry and distribution of anomalous plutonic belts in the batholiths of California: effects of assimilation, cratonal thickness, and depth of crystallization. *Bull. geol. Soc. Am.* **100**, 912–927.

Anderson, J. R. 1983. Petrology of a portion of the Eastern Peninsular Ranges mylonite zone, southern California. *Contrib. Mineral. Petrol.* **84**, 253–271.

Behrmann, J. H. & Mainprice, D. 1987. Deformation mechanisms in a high-temperature quartz feldspar mylonite: evidence for superplastic flow in the lower continental crust. *Tectonophysics* **140**, 297–305.

Bell, I. A. & Wilson, C. J. L. 1977. Growth defects in metamorphic biotite. *Phys. Chem. Miner.* **2**, 153–169.

Berthé, M. G., Choukroune, P. & Jegouzo, P. 1979. Orthogneiss, mylonite and non-coaxial deformation of granites: the example of the South Armorican shear zone. *J. Struct. Geol.* **1**, 31–42.

Boullier, A. M. & Guegen, Y. 1975. SP-mylonites: Origin of some mylonites by superplastic flow. *Contrib. Mineral. Petrol.* **23**, 128–135.

Burg, J.-P. & Laurent, Ph. 1978. Strain analysis of a shear zone in a granodiorite. *Tectonophysics* **47**, 15–42.

Christoffersen, R. & Kronenberg, A. K. 1993. Dislocation interactions in experimentally deformed biotite. *J. Struct. Geol.* **15**, 1077–1095.

Dokka, R. K. 1984. Fission-track geochronologic evidence for Late Cretaceous mylonitization and early Paleocene uplift of the northeastern Peninsular Ranges, California. *Geophys. Res. Lett.* **11**, 46–49.

Erskine, B. G. 1985. Mylonitic deformation and associated low-angle faulting in the Santa Rosa mylonite zone, southern California. Unpublished Ph.D. thesis, University of California, Berkeley, California.

Erskine, B. G. 1986a. Metamorphic and deformation history of the eastern Peninsular Ranges mylonite zone: Implications on tectonic reconstructions of southern California. *Geol. Soc. Am. Abs. w. Prog.* **18**, 105.

Erskine, B. G. 1986b. Syn-tectonic granitic intrusion and mylonitic deformation along the eastern margin of the northern Peninsular Ranges batholith southern California. *Geol. Soc. Am. Abs. w. Prog.* **18**, 105.

Erskine, B. G. & Wenk, H.-R. 1985. Evidence for late Cretaceous crustal thinning in the Santa Rosa mylonite zone, southern California. *Geology* **13**, 274–277.

Etheridge, M. A. & Wilkie, J. C. 1979. Grain size reduction, grain boundary sliding and the flow strength of mylonites. *Tectonophysics* **58**, 159–178.

Gapais, D. & White, S. H. 1982. Ductile shear bands in a naturally deformed quartzite. *Textures and Microstuctures* **5**, 1–17.

Gifkins, R. C. 1976. The effect of grain size and stress upon grain-boundary sliding. *Trans. Metall. A* **8A**, 1507–1516.

Goodwin, L. B. & Renne, P. R. 1991. Effects of progressive mylonitization on Ar retention in biotites from the Santa Rosa Mylonite Zone, California, and thermochronologic implications. *Contrib. Mineral. Petrol.* **108**, 283–297.

Goodwin, L. B. & Wenk, H.-R. 1990. Intracrystalline folding and cataclasis in biotite of the Santa Rosa mylonite zone: HVEM and TEM observations. *Tectonophysics* **172**, 201–214.

Hammarstrom, J. M. & Zen, E-An. 1988. Aluminum in hornblende: An empirical igneous geobarometer. *Am. Miner.* **71**, 1297–1313.

Handy, M. R. 1989. Deformation regimes and the rheological evolution of fault zones in the lithosphere: the effects of pressure, temperature, grain size and time. *Tectonophysics* **163**, 119–152.

Helming, K., Wenk, H.-R., Choi, C. S. & Schafer, W. 1994. Description of quartz textures by components. Examples from metamorphic rocks. In: *Textures of Geological Materials* (edited by Bunge, H. J., Siegesmund, S., Skrotzki, W. & Webber, K.). DGM Informationgesellschaft, Oberursel, Germany.

Jiang, D. 1994a. Vorticity determination, distribution, partitioning and the heterogeneity and non-steadiness of natural deformations. *J. Struct. Geol.* **16**, 121–130.

Jiang, D. 1994b. Flow variation in layered rocks subjected to bulk flow of various kinematic vorticities: theory and geological implications. *J. Struct. Geol.* **16**, 1159–1172.

Jiang, D. & White, J. C. In press. The heterogeneity and non-steadiness of natural flow: Implications for kinematic interpretations and inferred deformation paths. *EOS.*

Jones, K. A. & Galwey, A. K. 1972. Variation of the length/thickness ratio of biotite crystals in metamorphic rocks. *J. Geol.* **80**, 112–120.

Kirby, S. H. 1985. Rock mechanics observations pertinent to the rheology of the continental lithosphere and the localization of strain along shear zones. *Tectonophysics* **119**, 1–27.

Kirby, S. H. & Kronenberg, A. K. 1987. Rheology of the lithosphere: Selected topics. *Rev. Geophys.* **25**, 1219–1244.

Knipe, R. J. 1989. Deformation mechanisms—recognition from natural tectonites. *J. Struct. Geol.* **11**, 127–146.

Knopf, E. B. 1931. Retrogressive metamorphism and phyllonitization. *Am. J. Sci.* **21**, 1–27.

Kronenberg, A. K., Kirby, S. H. & Pinkston, J. 1990. Basal slip and mechanical anisotropy of biotite. *J. geophys. Res.* **B95**, 19,257–19,278.

Lapworth, C. 1885. The Highland controversy in British geology: its causes, course, and consequences. *Nature* **32**, 558–559.

Means, W. D. 1989. Synkinematic microscopy of transparent polycrystals. *J. Struct. Geol.* **11**, 163–174.

O'Brien, D. K. 1985. Strain estimation and sense-of-shear determination in phyllonites and ultramylonites based on phyllosilicate preferred orientation. M.S. Thesis, University of California at Berkeley, Berkeley, California.

O'Brien, D. K., Wenk, H.-R., Ratschbacher, L. & You, Z. 1987. Preferred orientation of phyllosilicates in phyllonites and ultramylonites. *J. Struct. Geol.* **9**, 719–730.

O'Hara, K. 1988. Fluid flow and volume loss during mylonitization: an origin for phyllonite in an overthrust setting, North Carolina, U.S.A. *Tectonophysics* **156**, 12–36.

Paterson, M. S. 1979. Brittle–ductile transition. In: *Experimental Rock Deformation: The Brittle Field* (edited by Paterson, M. S.). Springer-Verlag, Berlin/Heidelberg, 161–187.

Paterson, S. R., Vernon, R. H. & Tobisch, O. T. 1989. A review of criteria for the identification of magmatic and tectonic foliations in granitoids. *J. Struct. Geol.* **11**, 349–363.

Platt, J. P. 1979. Extensional crenulation cleavage. *J. Struct. Geol.* **1**, 95.

Platt, J. P. & Vissers, R. L. M. 1980. Extensional structures in anisotropic rocks. *J. Struct. Geol.* **2**, 397–410.

Ponce de Leon, M. J. & Choukroune, P. 1980. Shear zones in the Iberian arc. *J. Struct. Geol.* **2**, 63–68.

Ramsay, J. G. 1980. Shear zone geometry: a review. *J. Struct. Geol.* **2**, 83–99.

Ramsay, J. G. & Graham, R. H. 1970. Strain variation in shear belts. *Can. J. Earth Sci.* **7**, 786–813.

Sander, B. 1911. Über Susammenhänge zwichen Teilbewegungen und Gefüge in Gesteinen. *Tschermaks mineralog. petrog. Mitt.* **30**, 281–314.

Segall, P. & Simpson, C. 1986. Nucleation of ductile shear zones on dilatant fractures. *Geology* **14**, 56–59.

Sharp, R. V. 1967. San Jacinto fault zone in the Peninsular Ranges of southern California. *Bull. geol. Soc. Am.* **78**, 705–730.

Sharp, R. V. 1979. Some characteristics of the eastern Peninsular Ranges mylonite zone. In: *Proc. Conf. VIII, Analysis of Actual Fault Zones in Bedrock*. U.S. Geological Survey Open-File Report **79-1239**, 258–267.

Sibson, R. H. 1977. Fault rocks and fault mechanisms. *J. geol. Soc. Lond.* **133**, 191–213.

Sibson, R. H. 1986. Earthquakes and rock deformation in crustal fault zones. *Ann. Rev. Earth & Planet. Sci.* **14**, 149–175.

Simpson, C. 1982. Strain and shape fabric variations associated with ductile shear zones. *J. Struct. Geol.* **2**, 165–171.

Simpson, C. 1984. Borrego Springs–Santa Rosa mylonite zone: A Late Cretaceous west-directed thrust in southern California. *Geology* **12**, 8–11.

Simpson, C. 1985. Deformation of granitic rocks across the ductile–brittle transition. *J. Struct. Geol.* **7**, 503–511.

Smith, J. V. & Yoder, H. S. Jr. 1956. Experimental and theoretical studies of the mica polymorphs. *Mineralog. Mag.* **31**, 209–235.

Theodore, T. G. 1970. Petrogenesis of mylonites of high metamorphic grade in the Peninsular Ranges of southern California. *Bull. geol. Soc. Am.* **81**, 435–450.

Todd, V. R., Erskine, B. G. & Morton, D. M. 1988. Metamorphic and tectonic evolution of the northern Peninsular Ranges batholith, southern California. In: *Metamorphic and Crustal Evolution of the Northern Peninsular Ranges Batholith, Southern California* (edited by Ernst, W. G.). Rubey Volume no., VII, Prentice-Hall, Englewood Cliffs, New Jersey.

Tullis, J., Dell'Angelo, L. & Yund, R. A. 1990. Ductile shear zones from brittle precursors in feldspathic rocks: the role of dynamic recrystallization. In: *The Brittle–Ductile Transition in Rocks* (edited by Duba, A., Durham, W., Handin, J. & Wang, H.). *A.G.U. Geophysical Monograph* **56**, Washington, D.C., 67–81.

Tullis, J., Snoke, A. W. & Todd, V. R. 1982. Significance and petrogenesis of mylonitic rocks. Penrose Conference Report. *Geology* **10**, 227–230.

Twiss, R. J. 1977. Theory and applicability of a recrystallized grain size paleopiezometer. *Pure & Appl. Geophys.* **115**, 227–244.

Vernon, R. H. 1984. Restite, xenoliths and microgranitoid enclaves in granites. *Nature* **309**, 438–439.

Vernon, R. H., Etheridge, M. A. & Wall, V. J. 1988. Shape and microstructure of microgranitoid enclaves: indicators of magma mingling and flow. *Lithos* **22**, 1–11.

Wenk, H.-R. & Pannetier, J. 1990. Texture development in deformed granodiorites from the Santa Rosa mylonite zone, southern California. *J. Struct. Geol.* **12**, 177–184.

White, S. H., Burrows, S. E., Carreras, J., Shaw, N. D. & Humphreys, F. J. 1980. On mylonites in ductile shear zones. *J. Struct. Geol.* **2**, 175–187.